Model for nonlinear behavior in the self-amplified spontaneous-emission free-electron laser

S. Krinsky
Brookhaven National Laboratory, Upton, New York 11973, USA
(Received 8 December 2003; published 10 June 2004)

We introduce a simplified model for the saturation of a self-amplified spontaneous-emission free-electron laser. Within this model, we determine the effect of nonlinearity upon the statistical properties of the output radiation. Comparing our results with the computer simulations of Saldin, Schneidmiller, and Yurkov [*The Physics of Free Electron Lasers* (Springer-Verlag, Berlin, 2000)], we find that the model provides a good description of the average intensity, field correlation function, and coherence time, but underestimates the intensity fluctuation. Asymmetric spectral broadening phenomena are not included in the model.

DOI: 10.1103/PhysRevE.69.066503 PACS number(s): 41.60.Cr, 05.40.−a, 02.50.−r

I. INTRODUCTION

The self-amplified spontaneous-emission free-electron laser (SASE FEL) starts up from the shot noise in the electron beam [1–4]. The output is narrow-band chaotic radiation and requires a statistical description. In the linear region of exponential growth [1–7] before saturation, the statistics are determined from the Central Limit Theorem [1,4]. In the nonlinear saturation region, the statistics are not so easily described. A comprehensive and illuminating study [1] of the nonlinear statistics was carried out by numerical solution of the time-dependent FEL equations. In this paper, we consider a simplified model for the nonlinear stochastic SASE field and compare its predictions with the results of Ref. [1]. In this model, the statistical properties of the nonlinear field are expressed in terms of those of the linear field. The model provides a good description of the average intensity, field correlation function, and coherence time, but it underestimates the intensity fluctuation. Asymmetric spectral broadening phenomena are not included in the model.

Ignoring the transverse dependence, the SASE electric field can be expressed in the form

$$E(z,t) = A(z,t)\exp\left(ik_r z - i\omega_r t\right), \tag{1.1}$$

where z represents the location along the undulator at which the SASE is observed and t represents the temporal position in the radiation pulse. For an undulator with period $\lambda_u = 2\pi/k_u$ and magnetic field strength parameter K, the resonant frequency is

$$\omega_r = k_r c = \frac{2k_u c\gamma^2}{1+K^2/2}. \tag{1.2}$$

In the linear region before saturation, the SASE power increases exponentially [1–7] and the slowly varying amplitude can be approximated by [2,3]

$$A_L(z,t) = A_0(z)\sum_{j=1}^{N_e}\exp\left[i\omega_r t_j - \frac{\left(t-t_j-z/v_g\right)^2}{4\sigma_t^2}\left(1+\frac{i}{\sqrt{3}}\right)\right]. \tag{1.3}$$

Here, N_e is the total number of electrons in the bunch, $A_0(z)$ contains the exponential growth factor, $0 \leqslant t_j \leqslant T_b$ is the random arrival time of the jth electron, cT_b is the electron bunch length, and v_g is the group velocity of each wave packet. The characteristic wave packet width $\sigma_t = 1/(\sqrt{3}\sigma_\omega)$, where $\sigma_\omega = \omega_r\sqrt{3\sqrt{3}\rho/k_u z}$ is the SASE bandwidth [2,3] and ρ the FEL parameter [7]. The coherence time [1,4] is $T_{coh} = \sqrt{\pi}/\sigma_\omega = \sqrt{3\pi}\sigma_t$. In this paper, we are considering a flat-top electron bunch with duration $T_b \gg T_{coh}$, and we use the dimensionless distance $Z = 2\rho k_u z$, time $\tau = 2\rho[(k_r + k_u)z - \omega_r t]$, and amplitude $A \equiv E/\sqrt{\rho n_0 \gamma_0 mc^2/\varepsilon_0}$ (mks units), where n_0 is the electron density and γ_0 the electron energy in units of the rest mass.

In the case of a monochromatic input wave (Sec. II), the amplified output field has the form [8]

$$A(Z) \cong A_L(Z)h\left[|A_L(Z)|^2\right] \quad (Z \gg 1), \tag{1.4}$$

where

$$A_L(Z) = \frac{1}{3}A(0)\exp\left[\left(\frac{\sqrt{3}}{2}+\frac{i}{2}\right)Z\right] \tag{1.5}$$

is the solution to the linearized single frequency equations. The initial value of the radiation field is assumed to be small, i.e., $A(0) \ll 1$.

In this paper, we introduce a simplified model (Sec. III) for SASE saturation by considering an ansatz for the nonlinear radiation field, expressing it in terms of the linear SASE field via

$$A(Z,\tau) \cong A_L(Z,\tau)h\left[|A_L(Z,\tau)|^2\right] \quad (Z \gg 1), \tag{1.6}$$

where $A_L(Z,\tau)$ is the linear approximation (1.3) to the SASE amplitude. The function $h(\xi)$ is that appearing in Eq. (1.4) and it can be evaluated by direct numerical integration of the single frequency FEL equations (see Sec. II). The model SASE intensity is

$$|A(Z,\tau)|^2 \cong I\left[|A_L(Z,\tau)|^2\right] \quad (Z \gg 1), \tag{1.7}$$

where $I(\xi) = \xi|h(\xi)|^2$. From Eqs. (1.6) and (1.7), the statistical properties of the nonlinear SASE field can be determined in terms of the known statistical properties [1,4] of the linear approximation $A_L(Z,\tau)$.

Whereas the scaling relation (1.4) for amplification of a monochromatic wave is a precise asymptotic relation for large Z, the ansatz (1.6) for SASE relies on an additional

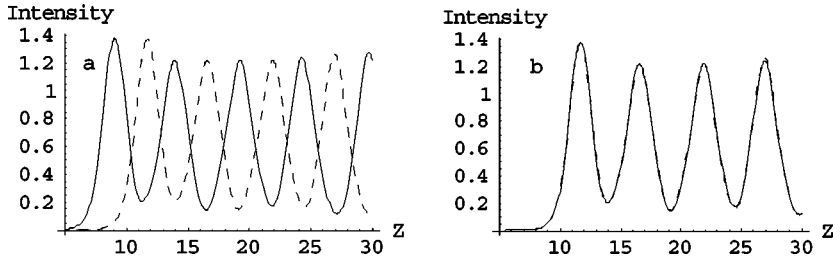

FIG. 1. (a) The dimensionless intensity $|A(Z)|^2$, as computed from the numerical solution of Eqs. (2.1)–(2.3) for the two initial conditions: $A(0)=.003$ (solid) and $A(0)=.0003$ (dashed), versus the dimensionless distance Z. (b) The solid curve in (a) has been translated to the right by $\Delta Z=2.658$ and now lies precisely over the dashed curve, as predicted by the scaling relation of Eq. (2.4).

approximation of limited validity. Slippage is taken into account in the linear approximation $A_L(Z,\tau)$, but not in the function $h(\xi)$ describing saturation. Some justification for using our model to describe the initial saturation process is as follows: Early in saturation, the SASE pulse is comprised of temporal spikes [9] having widths equal to a few cooperation lengths $(\lambda_r/4\pi\rho)$. The field amplitude at this point is still accurately described by the linear approximation. As the electrons travel several more gain lengths down the undulator, the additional slippage is on the order of the coherence length, so that the energy transfer between the electrons and field may take place in a manner similar to the steady state case, and the ansatz (1.6) can provide a useful description. However, as the electrons continue further along the undulator, the slippage exceeds the original coherence length and the model can be expected to lose validity.

II. AMPLIFICATION OF THE MONOCHROMATIC WAVE

The scaled equations [7] for the evolution of a one-dimensional electron distribution and a monochromatic radiation field are

$$\frac{d\theta_j}{dZ}=p_j, \tag{2.1}$$

$$\frac{dp_j}{dZ}=-Ae^{i\theta_j}-A^*e^{-i\theta_j}, \tag{2.2}$$

$$\frac{dA}{dZ}=\langle e^{-i\theta_j}\rangle, \tag{2.3}$$

where $\theta_j=(k_r+k_w)z-\omega_r t_j(z)$ is the phase of the jth electron relative to the radiation and $p_j=(\gamma-\gamma_0)/\rho\gamma_0$ is its (scaled) energy deviation. The bracket represents an average over the electron phases in the interval $0\leqslant\theta_j\leqslant 2\pi$.

We have shown [8] (see Appendix A) that the solution to Eqs. (2.1)–(2.3) can be expressed in the form

$$A(Z)\cong A_L(Z)h\big[|A_L(Z)|^2\big] \quad (Z\gg 1), \tag{2.4}$$

where

$$A_L(Z)=\frac{1}{3}A(0)\exp\left[\left(\frac{\sqrt{3}}{2}+\frac{i}{2}\right)Z\right] \tag{2.5}$$

is the solution to the linearized single-frequency FEL equations. Equation (2.4) is valid as long as the initial value of the radiation field is small, $A(0)\ll 1$. The radiation intensity is given by

$$|A(\varepsilon,Z)|^2\cong I(\xi)\equiv\xi|h(\xi)|^2 \quad (Z\gg 1), \tag{2.6}$$

where

$$\xi\equiv\frac{1}{9}A(0)^2\,e^{\sqrt{3}Z}. \tag{2.7}$$

It follows from Eq. (2.6) that for large Z, the intensity does not depend on $A(0)$ and Z independently, but only in the combination specified in Eq. (2.7). Therefore, a change in the initial value of the radiation field $[A(0)]$ corresponds to a translation in Z. The validity of this scaling is demonstrated in Fig. 1, where we plot the intensity determined from the numerical solution of the FEL Eqs. (2.1)–(2.3) for two initial conditions $A(0)=.0003$ and $A(0)=.003$. The equations were solved numerically using MATHEMATICA with 1000 electrons, initially equally spaced in phase in the interval $0\leqslant\theta_j\leqslant 2\pi$. It is seen that once the exponential gain has been established, the two intensities differ only by a translation in Z by $Z_1-Z_2=(2/\sqrt{3})\ln[A_2(0)/A_1(0)]=2.658$.

The function $h(\xi)$ can be evaluated by direct numerical integration of the single frequency equations. Let $A_{sf}(Z)$ be the solution of Eqs. (2.1)–(2.3) for the initial condition $A_{sf}(0)=\varepsilon_{sf}$. It follows that $\sqrt{\xi}\,h(\xi)=A_{sf}[Z_0(\xi)]\times\exp[-iZ_0(\xi)/2]$, with $Z_0(\xi)=[\ln\xi+\ln(9/\varepsilon_{sf}^2)]/\sqrt{3}$. In Fig. 2, we plot the magnitude and phase of the function h.

III. MODEL FOR NONLINEAR SASE STATISTICS

The simplified model for SASE saturation is defined by the ansatz for the nonlinear radiation field

$$A(Z,\tau)\cong A_L(Z,\tau)h\big[|A_L(Z,\tau)|^2\big] \quad (Z\gg 1), \tag{3.1}$$

where $A_L(Z,\tau)$ is the linear approximation (1.3) to the SASE amplitude. The function $h(\xi)$ is that presented in Fig. 2, determined by direct numerical integration of the single frequency FEL equations. The model SASE intensity is

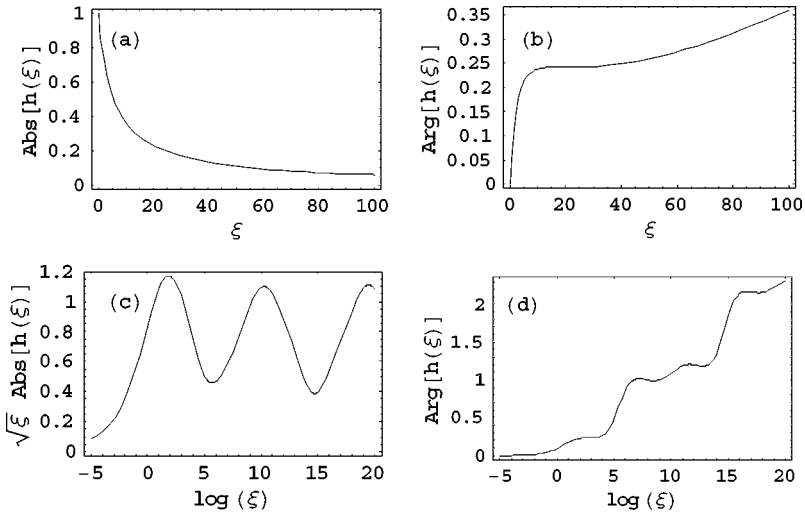

FIG. 2. We plot (a) the magnitude and (b) the phase of the scaling function $h(\xi)$ versus ξ. In order to show the behavior over a wider domain, we plot (c) $\sqrt{\xi}|h(\xi)|$ and (d) $\arg[h(\xi)]$ versus the natural $\log(\xi)$.

$$|A(Z,\tau)|^2 \cong I\left[|A_L(Z,\tau)|^2\right] \quad (Z \gg 1), \tag{3.2}$$

where $I(\xi)$ is defined in Eq. (2.6) and can also be evaluated by integrating the single frequency FEL equations. From Eqs. (3.1) and (3.2), the statistical properties of the nonlinear SASE field can be determined in terms of the known statistical properties [1,4] of the linear approximation $A_L(Z,\tau)$.

Within the linear approximation, the field correlation is given by

$$\left\langle A_L(Z,\tau_1)A_L^*(Z,\tau_2)\right\rangle \cong i_{av}(Z)\exp\left[\frac{-\pi(\tau_1-\tau_2)^2}{2\tau_c^2(Z)}\right], \tag{3.3}$$

where

$$i_{av}(Z) = \left\langle |A(Z,\tau)|^2\right\rangle \cong \frac{\exp\left(\sqrt{3}Z\right)}{9\sqrt{2}\,N_c\tau_c(Z)} \tag{3.4}$$

is the average intensity and

$$\tau_c(Z) = \sqrt{2\pi Z/\left(3\sqrt{3}\right)} \tag{3.5}$$

the coherence time. N_c is the number of electrons in a cooperation length $\lambda_r/4\pi\rho$. The brackets $\langle\ \rangle$ represent the average over the electron arrival times (shot noise).

Since the SASE intensity in the linear regime is described by the exponential distribution [1], $(1/\langle I\rangle)\exp(-I/\langle I\rangle)$, we can use Eq. (3.2) to express the average of the nth power of the nonlinear SASE intensity in the form

$$\left\langle |A(Z,\tau)|^{2n}\right\rangle = \int dQ\,\exp(-Q)I^n[Qi_{av}(Z)]. \tag{3.6}$$

The intensity fluctuation is given by

$$\sigma_I^2(Z) = \frac{\left\langle |A(Z,\tau)|^4\right\rangle - \left\langle |A(Z,\tau)|^2\right\rangle^2}{\left\langle |A(Z,\tau)|^2\right\rangle^2}. \tag{3.7}$$

In Fig. 3, we plot the average intensity $\langle|A(Z,\tau)|^2\rangle$ versus Z, as determined from Eq. (3.6). In this figure and those that follow, we have chosen the number of electrons in a cooperation length to be $N_c=1.5\times10^7$. In Ref. [1], the definition of N_c is twice ours; hence, our $N_c=1.5\times10^7$ corresponds to their choice of $N_c=3\times10^7$. The intensity, shown as the solid curve in Fig. 1, is in good agreement with Fig. 6.13 of Ref. [1] out to about $Z=14$. After this point, their simulations are dominated by spectral broadening phenomena not included in the simplified model. The slight shift of our result to larger Z as compared with the result of Ref. [1], may be due to a difference in the treatment of shot noise in our analytic approximation and their numerical simulation. The intensity fluctuation $\sigma_I(Z)$ is presented in Fig. 4. There is significant disagreement in the results. The fluctuation at the intensity maximum (at $Z=13$) is about 25%, which is one-half of the value determined in the simulations (Fig. 6.15 of Ref. [1]). This is due to a limitation of our approximation, which will be discussed in more detail later.

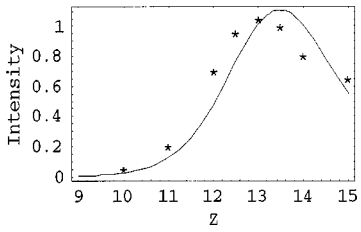

FIG. 3. The average dimensionless SASE intensity I (solid) as calculated from Eq. (3.6) with $n=1$. The stars represent values of the intensity read from Fig. 6.13 of Ref. [1].

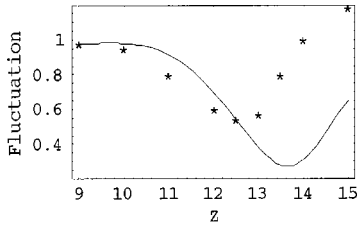

FIG. 4. The intensity fluctuation σ_I (solid) as determined from Eq. (3.7), plotted versus the dimensionless distance Z traveled along the undulator. The stars represent values of the fluctuation read from Fig. 6.15 of Ref. [1].

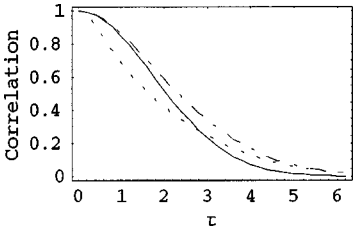

FIG. 5. The field correlation $g_1(Z,\tau)=\langle A(Z,0)A^*(Z,\tau)\rangle / \langle |A(Z,0)|^2\rangle$ as given in Eq. (3.8), plotted against dimensionless time τ, for dimensionless distance traveled along the undulator for $Z=8$ (solid), $Z=13$ (dot-dashed), and $Z=15$ (dashed).

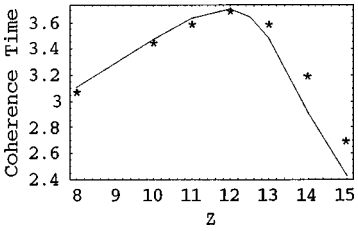

FIG. 6. The dimensionless coherence time $\tau_{coh}(Z)$ (solid curve) as computed from Eq. (3.11) plotted against the dimensionless distance Z traveled along the undulator. The stars represent (twice the) values read from Fig. 6.20 of Ref. [1].

The radiation field correlation function is given by (see Appendix B)

$$\begin{aligned}\langle A(Z,\tau_a)A^*(Z,\tau_b)\rangle &\equiv \langle |A(Z,0)|^2\rangle g_1(Z,\tau_a-\tau_b)\\ &= \int dQ_a dQ_b P_1(Q_a,Q_b,Z,\tau_a-\tau_b)\\ &\quad\times\sqrt{Q_a i_{a\nu}(Z) Q_b i_{a\nu}(Z)}\,h[Q_a i_{a\nu}(Z)]h^*[Q_b i_{a\nu}(Z)],\end{aligned} \tag{3.8}$$

where

$$P_1(Q_a,Q_b;Z,\tau_a-\tau_b)=\frac{\exp\left(\frac{-Q_a}{1-\beta_{ab}}\right)\exp\left(\frac{-Q_b}{1-\beta_{ab}}\right)}{1-\beta_{ab}} \times I_1\left(\frac{2\sqrt{\beta_{ab}Q_aQ_b}}{1-\beta_{ab}}\right), \tag{3.9}$$

$$\beta_{ab}\equiv\frac{\langle |A_L(Z,\tau_a)|^2|A_L(Z,\tau_b)|^2\rangle}{\langle |A_L(Z,\tau_a)|^2\rangle\langle |A_L(Z,\tau_b)|^2\rangle}-1\cong\exp\left[\frac{-\pi(\tau_a-\tau_b)^2}{\tau_c^2(Z)}\right]. \tag{3.10}$$

The integrand in Eq. (3.8) is symmetric in Q_a and Q_b, hence the model field correlation is real, whereas the precise result is a complex quantity. In Fig. 5, we show the field correlation before and during saturation. Our results are seen to agree with Figs. 6.16 and 6.17 of Ref. [1] upon noting that our definition of the scaled time τ is twice theirs.

Knowledge of the field correlation enables us to compute the coherence time [1] defined by

$$\tau_{coh}(Z)\equiv\int_{-\infty}^{\infty}d\tau|g_1(Z,\tau)|^2. \tag{3.11}$$

The coherence time is plotted in Fig. 6. The results are seen to be in good agreement with Fig. 6.20 of Ref. [1]. Note that our definition of τ_{coh} is twice theirs.

The normalized spectrum envelope [1] is given by

$$W(Z,\Omega)=\int_{-\infty}^{\infty}d\tau\, g_1(Z,\tau)e^{i\Omega\tau}, \tag{3.12}$$

where $W(Z,\Omega)d\Omega$ is the fraction of the total energy radiated (averaged over many pulses) in the frequency interval Ω to $\Omega+d\Omega$ at distance Z along the undulator. We plot the spectral envelope for $Z=8,13,15$ in Fig. 7. The normalized frequency deviation is defined by $\Omega\equiv(\omega-\omega_r)/2\rho\omega_r$. In the linear regime [Fig. 7(a)], the distribution has the exponential form

$$W(Z,\Omega)=\frac{1}{\sqrt{2\pi}\sigma_\Omega(Z)}\exp\left[\frac{-\Omega^2}{2\sigma_\Omega^2(Z)}\right], \tag{3.13}$$

where $\sigma_\Omega(Z)=\sqrt{\pi}/\tau_c(Z)$. Near the maximum of the average intensity [Fig. 7(b)], the distribution is narrower than case (a), while near the first intensity minimum [Fig. 7(c)], the distribution is broader exhibiting a slowly falling tail. In our model, the spectral broadening at saturation is symmetric, while in simulations it becomes asymmetric due to phenomena we have not included.

In order to determine the distribution of instantaneous intensity, we express the model in a form suitable for evaluation by numerical simulation. In the region of exponential gain before saturation, the linear SASE field can be expressed as in Eq. (1.3). We shall write

$$A_L(Z,\bar{t})\cong\frac{A_0}{\sqrt{Z/10}}\exp\left[\frac{\sqrt{3}}{2}(Z-10)\right] \times\sum_{j=i}^{N_e}\exp\left[i2\pi f_r\bar{t}_j-\frac{(\bar{t}-\bar{t}_j)^2}{4\bar{\sigma}_t^2(Z/10)}\left(1+\frac{i}{\sqrt{3}}\right)\right], \tag{3.14}$$

where $\bar{t}=t/T_b$ and $\bar{t}_j=t_j/T_b$ are random numbers uniformly distributed in the interval $0\leqslant\bar{t}_j\leqslant1$. We choose the parameters

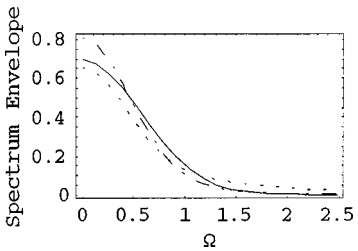

FIG. 7. The spectrum envelope $W(Z,\Omega)$, as given in Eq. (3.12), plotted against dimensionless frequency Ω, for dimensionless distance traveled along the undulator for $Z=8$ (solid), (b) $Z=13$ (dot-dashed), and (c) $Z=15$ (dashed).

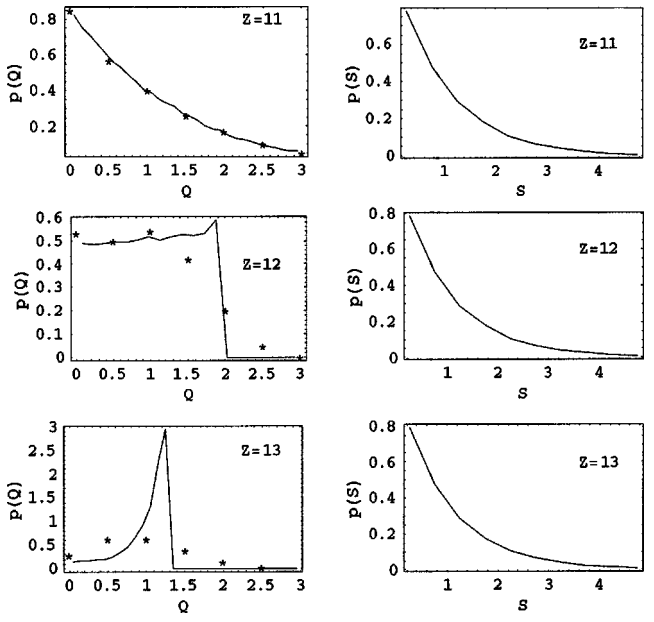

FIG. 8. Histograms $p(Q)$ and $p(S)$ of the normalized instantaneous intensity $Q=I(t)/\langle I\rangle$ and normalized spectral intensity $S=\tilde{I}(\omega)/\langle\tilde{I}(\omega)\rangle$, at positions $Z=11,12,13$ along the undulator. Stars represent values of the distribution of instantaneous intensity $p(Q)$ as read off of Fig. 6.14 of Ref [1].

$$N_e = 5000, \quad f_r \equiv \omega_r T_b/2\pi = 500.1, \quad \bar{\sigma}_t \equiv \sigma_t/T_b = 0.0035, \quad A_0 = 0.034.$$

An overall Z-dependent phase factor that does not affect our results is neglected. The value of the constant A_0 is determined by the condition that the linear intensity at $Z=10$ agrees with Eq. (3.4); i.e.,

$$\langle |A_L(10,t)|^2\rangle = A_0^2\sqrt{2\pi}N_e\bar{\sigma}_t = i_{a_v}(10) = 0.050. \quad (3.15)$$

The value of the FEL parameter ρ is found by requiring that the coherence time $\sqrt{3\pi}\sigma_t$ in the linear approximation be given by Eq. (3.5):

$$\tau_c(10) = 2\rho\omega_r T_b\bar{\sigma}_t\sqrt{3\pi} = \sqrt{\frac{20\pi}{3\sqrt{3}}}. \quad (3.16)$$

It follows that $2\rho=0.10$.

The nonlinear field A is determined from Eq. (3.1) in terms of the linear field A_L of Eq. (3.14). Choosing an ensemble of 500 sets of random numbers $\{\bar{t}_j, j=1,\ldots,N_e\}$, we simulate multiple SASE pulses. The numerical results obtained in this manner agree with the analytic results presented in Figs. 3–7. In addition, we have determined the distribution $p(Q)$ of the ratio of the instantaneous intensity to the average intensity $Q=I(t)/\langle I\rangle$, and the distribution $p(S)$ of the ratio of the spectral intensity to the average spectral intensity $S=\langle\tilde{I}(\omega)/\tilde{I}(\omega)\rangle$, for $Z=11,12,13$ (see Fig. 8). At $Z=11$, the distribution $p(Q)$ is close to the exponential form $\exp(-Q)$, which holds in the linear regime. At $Z=12$, the distribution deviates from exponential, with the smaller values of Q suppressed. The model distribution is in good agreement with Fig. 6.14 of Ref. [1]. At $Z=13$, the lower values of Q are more strongly suppressed than in the numerical simulations of Ref. [1] and the strict upper limit on the model intensity introduces an artificial cutoff at larger Q. This clearly illustrates the limitation on the validity of the model as one goes deeper into saturation.

One of the most striking results of Ref. [1] is that the intensity observed after a monochromator is described by the exponential distribution $p(S)=\exp(-S)$, even after saturation. This is also true in our model, as seen in Fig. 8. Before saturation, the Fourier transform of the radiation field is a sum of terms, each of which depends on the arrival time of a single electron. The exponential distribution is a consequence of the Central Limit Theorem. After saturation, the Fourier transform of the field is no longer a sum of terms depending on the arrival time of a single electron. However, it is comprised of a sum of terms, each one the contribution of a single temporal spike. Since the time of a spike is random, the Fourier transform of the field has the form of a sum of terms possessing a random phase relative to one another. If the number of spikes is large, then the Central Limit Theorem again predicts an exponential distribution. In the case of our simulation, each of the 500 pulses contains, on average, 65 temporal spikes.

IV. CONCLUSIONS

In the linear region before saturation, the statistical properties of the SASE radiation are determined from quite general considerations based on the Central Limit Theorem [1,4]. When the nonlinear effects associated with saturation are important, the Central Limit Theorem no longer applies and information on the statistical behavior comes from numerical solution [1] of the time-dependent FEL equations. In this paper, we have considered a model that provides a good approximation to the statistical behavior of SASE early in saturation. In this model, the statistical properties of the nonlinear field are expressed in terms of those of the linear field.

Whereas the scaling relation (1.4) for amplification of a monochromatic wave is a precise asymptotic relation for large Z, the model (1.6) for SASE relies on an additional approximation of limited validity. Slippage is taken into account in the linear approximation $A_L(Z,\tau)$, but not in the function $h(\xi)$ describing saturation. Some justification for using our model to describe the initial saturation process is as follows: Early in saturation, the SASE pulse is comprised of temporal spikes [9] having widths equal to a few cooperation lengths $(\lambda_r/4\pi\rho)$. The field amplitude at this point is still accurately described by the linear approximation. As the electrons travel several more gain lengths down the undulator, the additional slippage is on the order of the coherence length, so that the energy transfer between the electrons and field may take place in a manner similar to the steady state case, and the model (1.6) can provide a useful description. However, as the electrons continue further along the undulator, the slippage exceeds the original coherence length and the model can be expected to lose validity.

The model has no free parameters and provides a good description of the statistical properties of SASE early in satu-

ration. Agreement with numerical simulations based on the time-dependent FEL equations is found out to about $Z=14$ for the average intensity (Fig. 3), field correlation function (Fig. 5), and coherence time (Fig. 6), and out to about $Z=12$ for the distribution of normalized instantaneous intensity (Fig. 8). In saturation, the radiation observed after a monochromator continues to be described by the exponential distribution, as found in Ref. [1].

A key limitation of the model is that the peak spike intensity saturates at the "steady state" value given by the solution of the single-frequency equations. The model does not include effects due to frequency chirping [10] in the spikes, which make possible higher peak saturation values. As presently formulated, the model cannot describe the asymmetric broadening of the spectrum associated with the sideband instability.

ACKNOWLEDGMENTS

I wish to thank Dr. Z. Huang for enlightening comments and discussion of results from his time-dependent FEL code. I also wish to thank the Stanford Linear Accelerator Center for its hospitality during the course of this work. This work was supported by the U.S. Department of Energy, Contract Nos. DE-AC03-76SF00515 and DE-AC02-98CH10886.

APPENDIX A: DERIVATION OF SCALING EQUATION (1.4)

In Ref. [8], we derived the scaling equation (1.4) by expressing the solution of Eqs. (2.1)–(2.3) as a perturbation expansion in the small parameter ε, the initial value of the radiation amplitude $A(0)=\varepsilon$. We summarize the derivation in this Appendix. Without loss of generality, we consider $\varepsilon \ll 1$ to be real. Expanding in powers of ε, we write

$$\theta(Z,\theta_0,p_0) = \theta_0 + p_0 Z + \varepsilon\theta_1(Z,\theta_0,p_0) + \varepsilon^2\theta_2(Z,\theta_0,p_0) + \cdots, \tag{A1}$$

$$A(Z) = \varepsilon A_1(Z) + \varepsilon^3 A_3(Z) + \varepsilon^5 A_5(Z) + \cdots. \tag{A2}$$

The constraints $\theta_n(0)=\theta_n'(0)=0$, $(n\geqslant 1)$, and $A_1(0)=1$, $A_n(0)=0$, $(n\geqslant 3)$ assure that $\theta(0)=\theta_0$, $\theta'(0)=p_0$, and $A(0)=\varepsilon$. For an initially uniform, monoenergetic $(p_0=0)$ electron beam, and a monochromatic electromagnetic wave, the system is periodic, so that we can restrict our attention to the interval $0\leqslant\theta_0\leqslant 2\pi$. $\langle e^{-im\theta_0}\rangle=\delta_{m,0}$, where $\delta_{m,0}$ is the Kronecker delta which equals unity for $m=0$ and vanishes for all $m\neq 0$.

Equations (2.1)–(2.3) imply

$$\theta'' = -Ae^{i\theta} - A^* e^{-i\theta}, \tag{A3}$$

$$A''' - iA = iA^*\langle e^{-2i\theta}\rangle - \langle \theta'^2 e^{-i\theta}\rangle. \tag{A4}$$

The prime denotes the derivative with respect to Z. We insert the expansions of Eqs. (A1) and (A2) into Eqs. (A3) and (A4), and equate terms having equal powers of ε. The first-order amplitude has the well-known solution [1], $A_1(Z)=(e^{sZ}+e^{-s^*Z}+e^{-iZ})/3$, where $s=(\sqrt{3}+i)/2$. There are three modes: growing, decaying, and oscillating. For $Z\gg 1$, the exponentially growing mode dominates, i.e., $\varepsilon A_1(Z)\approx A_L(Z)\equiv(\varepsilon/3)\exp(sZ)$, and the perturbation coefficients θ_n and A_n have the form

$$\varepsilon^n\theta_n(Z,\theta_0) = \sum_{k=0}^{n} b(n,n-2k)A_L^{n-k}(Z)A_L^{*k}(Z)e^{i(n-2k)\theta_0} \quad (n\geqslant 1), \tag{A5}$$

and

$$\varepsilon^{2m+1}A_{2m+1}(Z) = a(m)A_L(Z)|A_L(Z)|^{2m} \quad (m\geqslant 0), \tag{A6}$$

where $b(n,n-2k)$ and $a(m)$ are complex constants independent of Z, determined recursively from Eqs. (A3) and (A4). We know that $a(0)=1$, we find θ_1,θ_2 from Eq. (A3) and A_3 from Eq. (A4). Next, θ_3,θ_4 are determined from Eq. (A3). Once this is accomplished, A_5 is found from Eq. (A4). In general, suppose we know $\theta_1,\theta_2,\ldots,\theta_{2m}$ and $A_1,A_3,\ldots,A_{2m+1}$, then θ_{2m+1} and θ_{2m+2} can be determined from Eq. (A3), and then A_{2m+3} can be found from Eq. (A4).

It is seen from Eqs. (A2) and (A6) that the radiation amplitude can be expressed in terms of the linear solution $A_L(Z)=(\varepsilon/3)\exp(sZ)$, as

$$A(Z;\varepsilon) \cong A_L(Z)h\left[|A_L(Z)|^2\right] \quad (Z\gg 1), \tag{A7}$$

with

$$h(\xi) = \sum_{m=0}^{\infty} a(m)\xi^m. \tag{A8}$$

Using MATHEMATICA, we have computed [8] the coefficients $a(1),\ldots,a(12)$ of the power series in Eq. (A8). It was found that after the first few values of n, the argument of the ratio $a(n)/a(n-1)$ remains close to 2.397 rad, and the magnitude of the ratio also varies slowly. The variation of the magnitude is further reduced if we multiply by $n/(n-1/2)$. These results suggest that there exists an inverse square root branch point at $\xi_0\cong\exp(-i2.397)/0.354$. This singularity limits the radius of convergence of the power series in Eq. (A8). Therefore, in order to use it to study saturation, we need to carry out an analytic continuation. In Ref. [8], we analytically continued the Taylor series by the use of Pade' approximate.

The numerical calculation of the first twelve coefficients suggest that the Taylor series in Eq. (8) has a finite radius of convergence and hence defines the function $h(\xi)$. This demonstrates the validity of the scaling relation (1.4).

APPENDIX B: DERIVATION OF EQ. (3.8)

In the linear regime, let us introduce the normalized field amplitude $a(Z,\tau)\equiv A_L(Z,\tau)/\sqrt{\langle|A_L(Z,\tau)|^2\rangle}$. The joint probability $p(x_a,y_a,x_b,y_b;Z,\tau_a-\tau_b)$ that the normalized amplitude has the values $a(Z,\tau_a)=x_a+iy_a=\sqrt{Q_a}\,e^{i\phi_a}$ and $a(Z,\tau_b)=x_b+iy_b=\sqrt{Q_b}\,e^{i\phi_b}$ at fixed position Z along the undulator, but at different times τ_a,τ_b, is given by [4]

$$p(x_a,y_a,x_b,y_b;Z,\tau_a-\tau_b) = \frac{1}{\pi^2(1-\beta_{ab})}\exp\left[\frac{-x_a^2-y_a^2-x_b^2-y_b^2+2u_{ab}(x_ax_b+y_ay_b)+2v_{ab}(x_ay_b-x_by_a)}{1-\beta_{ab}}\right], \tag{B1}$$

where

$$\langle a(Z,\tau_a)a^*(Z,\tau_b)\rangle = u_{ab}+iv_{ab} = \sqrt{\beta_{ab}}\,e^{i\psi_{ab}}. \tag{B2}$$

Using the approximate expression of Eq. (3.1) for the nonlinear field amplitude, the correlation function can be written in the form

$$\langle A(Z,\tau_a)A^*(Z,\tau_b)\rangle = \int dx_a dy_a dx_b dy_b p(x_a,y_a,x_b,y_b;Z,\tau_a-\tau_b) \times i_{av}(Z)\sqrt{Q_aQ_b}\,e^{i(\phi_a-\phi_b)}h[i_{av}(Z)Q_a]h^*[i_{av}(Z)Q_b], \tag{B3}$$

where $i_{av}(Z)$ is the average intensity in the linear approximation, given in Eq. (3.4). We change the integration variables to Q_a, Q_b, ϕ_a, ϕ_b, and carry out the integrations in (B3) over the phase angles to obtain Eq. (3.8):

$$\langle A(Z,\tau_a)A^*(Z,\tau_b)\rangle = e^{i\psi_{ab}}\int dQ_a dQ_b P_1(Q_a,Q_b;Z,\tau_a-\tau_b) \times\sqrt{Q_ai_{av}(Z)Q_bi_{av}(Z)}\,h[Q_ai_{av}(Z)]h^*[Q_bi_{av}(Z)], \tag{B4}$$

where P_1 was defined in Eq. (3.9). When β_{ab} is approximated by Eq. (3.10), $\psi_{ab}=0$.

[1] E.L. Saldin, E.A. Schneidmiller, and M.V. Yurkov, *The Physics of Free Electron Lasers* (Springer-Verlag, Berlin, 2000).

[2] J.M. Wang and L.H. Yu, Nucl. Instrum. Methods Phys. Res. A **250**, 484 (1986).

[3] K.J. Kim, Nucl. Instrum. Methods Phys. Res. A **250**, 396 (1986).

[4] S. Krinsky and R.L. Gluckstern, Phys. Rev. ST Accel. Beams **6** 050701 (2003).

[5] N.M. Kroll and W.A. McMullin, Phys. Rev. A **17**, 300 (1978).

[6] Y.S. Debenev, A.M. Kondratenko, and E.L. Saldin, Nucl. Instrum. Methods Phys. Res. **193**, 415 (1982).

[7] R. Bonifacio, C. Pellegrini, and L.M. Narducci, Opt. Commun. **50**, 373 (1984).

[8] S. Krinsky, in Proc. FEL 2003, Tsukuba, Japan, 2003 ; see also SLAC-PUB-9619, http://www.slac.stanford.edu/cgi-wrap/getdoc/slac-pub-9619.pdf.

[9] R. Bonifacio, L. De Salvo, P. Pierini, N. Piovella, and C. Pellegrini, Phys. Rev. Lett. **73**, 70 (1994).

[10] R.W. Warren, J.C. Goldstein, and B.E. Newman, Nucl. Instrum. Methods Phys. Res. A **250**, 19 (1986).